ChemPlusChem

A Multidisciplinary Journal Centering on Chemistry

Chemistry Europe

European Chemical Societies Publishing

# Accepted Article

**Title:** Fine-Tuning Plasmon-Molecule Interactions in Gold-BODIPY Nanocomposites: The Role of Chemical Structure and Noncovalent Interactions

**Authors:** P.P Praveen Kumar, Atikur Rahman, Tanmay Goswami, Hirendra N. Ghosh, and Prakash P Neelakandan



**To be cited as:** *ChemPlusChem* 10.1002/cplu.202000545

**Link to VoR:** https://doi.org/10.1002/cplu.202000545

WILEY-VCH

WILEY-VCH

FULL PAPER

# Fine-Tuning Plasmon-Molecule Interactions in Gold-BODIPY Nanocomposites: The Role of Chemical Structure and Noncovalent Interactions

P. P. Praveen Kumar,[a]+ Atikur Rahman,[a]+ Tanmay Goswami,[a] Hirendra N. Ghosh*[a, b] and Prakash P. Neelakandan*[a]

[a] Dr. P. P. P. Kumar,+ A. Rahman,+ T. Goswami, Prof. H. N. Ghosh, Dr. P. P. Neelakandan
Institute of Nano Science and Technology, Habitat Centre, Phase 10, Sector 64, Mohali 160062 (India)
E-mail: hnghosh@inst.ac.in, ppn@inst.ac.in
[b] Prof. H. N. Ghosh
Radiation and Photochemistry Division, Bhabha Atomic Research Centre, Mumbai 400085 (India)
[+] *The authors P. P. P. Kumar and A. Rahman contributed equally to this article.*

Supporting information for this article is given via a link at the end of the document.

**Abstract:** Strong coupling between localized surface plasmons and molecular absorptions leads to remarkable changes in the photophysical properties of dye-loaded metal nanoparticles. Here, we report supramolecular nanocomposites consisting of BODIPY, tryptophan and gold nanoparticles and investigate the effect of structural variations on their photophysical properties. Our results indicate that the photostability and photosensitization properties of the nanocomposites depend on the chemical composition of the BODIPY molecules. The singlet oxygen quantum yield of the nanocomposites **NC1** and **NC3** were 0.46 and 0.42, respectively, which were significantly higher as compared to their individual components. Ultrafast spectroscopy studies revealed that the migration of photoexcited BODIPY electrons to the plasmonic photoexcitation allowed electron transfer into the singlet oxygen states thereby leading to efficient generation of singlet oxygen.

## Introduction

Plasmon-molecule coupling has emerged as a new modality for the development of photonic devices and optically responsive materials.[1–6] Metallic nanoparticles in combination with molecular adsorbates (dyes) provide a platform to construct heterostructures or "hybrid" materials whose photophysical properties may be tuned at the nanoscale.[7–10] Molecules which absorbs light near to the surface plasmon resonance (SPR) absorption peak of metal nanoparticles can induce changes in the photophysical and electronic properties of metal nanoparticles (MNPs) due to plasmon-molecule interactions.[11–17] Initial studies indicated that the coupling strength is directly proportional to the spectral overlap between the molecular and plasmonic resonances and thus can be fine-tuned by varying the molecule, its concentration and the size and shape of the MNPs.[18–21]

Interaction of several dye molecules with MNPs have been studied in the recent past.[22–28] Plasmon-molecule interactions are typically studied through steady-state spectroscopy measurements and supported by theoretical calculations. Ultrafast spectroscopy measurements would enable the characterization of the hybrid states, but such detailed studies are rarely taken up.[29–34] Halas and co-workers studied the ultrafast optical dynamics of a hybrid plasmon-exciton system consisting of a complex of *J*-aggregates of a thiacarbocyanine dye with gold nanoshells.[9] It was observed that the localized plasmons of the nanoshell coupled strongly with the excitons of the *J*-aggregates leading to a well-defined Fano resonance in the absorption spectrum of the complex. A combined one-exciton and two-exciton state models were evoked to describe the optical properties of the complex. Zhang, Wang and co-workers studied the strong coupling interactions between gold nanorods and the NIR dye IR-806.[31] It was observed that a prominent absorption dip occurred as the concentration of the dye increased and was saturated when one monolayer of the dye was formed on the surface. It was established that a unidirectional energy transfer occurred from the plasmons to the excitons and further allowed one-photon nonlinearity to be tuned. The results have been interpreted on the basis of saturated plasmonic absorption and weakened destructive Fano interference from the bleached excitonic absorption.

Although these studies provide insights into the underlying mechanism of plasmon-molecule coupling, it is impossible to generalize these mechanisms as only a few of examples are known. Moreover, systematic studies correlating the effect of chemical structure and functional groups on plasmon-molecule interactions are lacking. Recently, we reported a three-component nanocomposite consisting of tryptophan, BODIPY and gold nanoparticles.[35] It was observed that tryptophan and BODIPY were non-covalently attached onto the surface of gold nanoparticles and led to major changes in their photophysical properties. Owing to the excellent singlet oxygen generation efficiency of the nanocomposite, it exhibited photocytotoxicity against cancer cells. Here, we investigate the effect of chemical composition on the stability and photophysical properties of nanocomposites **NC1**-**NC5** (Figure 1) by using a series of BODIPY molecules wherein their structure was varied systematically. Our results indicate that sterically bulky molecules

tend to destabilize the nanocomposites. Further, detailed ultrafast spectroscopy studies was used to elucidate the mechanism of the coupling between the molecular and plasmonic resonances and the singlet oxygen generation.

## Results and Discussion

BODIPY molecules **B1-B5** used in the present study were synthesized as per literature procedures[36–39] and were characterized by NMR and mass spectrometry (Figures S1-S5). Nanocomposites **NC1-NC5** were prepared as reported earlier[35] wherein a BODIPY molecule (**B1-B5**) in acetone was added to a stirred aqueous solution of L-tryptophan (**Trp**) and $HAuCl_4$. The precipitated nanocomposites (**NC1-NC5**) were collected, purified by washing with water and characterized by transmission electron microscopy (TEM) and dynamic light scattering (DLS) (Figures S6-S7). The nanocomposites were found to be spherical in shape with an average diameter of 97 ± 3, 66 ± 3, 70 ± 2, 60 ± 3 and 57 ± 3 nm, respectively for **NC1-NC5**. We also prepared simple gold nanoparticles (**Au NP**) and organic nanoparticles (**ONP1-ONP5**) as reference materials. **Au NP**, which was prepared from $HAuCl_4$ using tryptophan as the reducing and capping agent, showed an average particle size of 35 ± 3 nm whereas **ONP1-ONP5** synthesized from **B1-B5**, respectively showed average particle size of 92 ± 3, 147 ± 4, 190 ± 3, 158 ± 3 and 187 ± 4 nm (Figure S8).

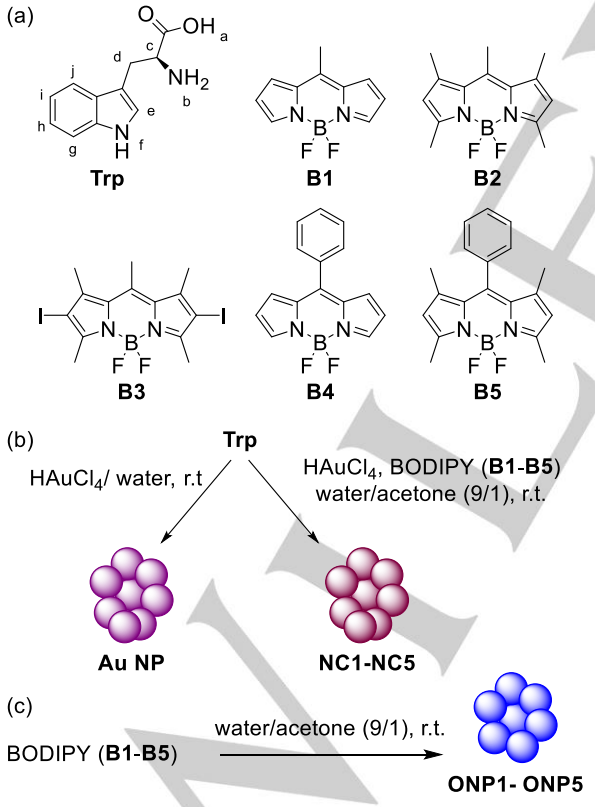


**Figure 1**. (a) Chemical structures of L-Tryptophan (**Trp**) and the BODIPY dyes **B1**-**B5**. General scheme for the synthesis of (b) tryptophan capped gold nanoparticles (**Au NP**) and the nanocomposites **NC1-NC5** and (c) organic nanoparticles **ONP1-ONP5**.

It is to be noted that the nanocomposite **NC5** synthesized from **B5** – the bulkiest of all BODIPYs used herein – behaved strangely: there were inconsistencies in the size of the nanocomposites obtained from different batches and their absorption spectra could not be reproduced (Figure S9). The peculiar behavior of **NC5** indicates the role of structural features in the nanocomposite formation. Owing to the steric hindrance imposed by the bulky methyl and phenyl groups, **B5** does not interact efficiently with gold thereby resulting in unstable nanocomposites. Because of the ambiguity in the structure of **NC5**, it was not used for further studies.

At the outset, we were interested in studying the steady-state absorption and emission features of the molecules **B1-B5**, organic nanoparticles **ONP1-ONP5** and the gold nanocomposites **NC1-NC4** (Figures 2, S10-S12 and Table 1). The photophysical properties of the molecules **B1-B5** in acetonitrile were typical of the BODIPY chromophore with sharp absorption and emission peaks and high fluorescence quantum yields. The BODIPY dyes **B1-B5** showed absorption peaks at 495, 490, 520, 496 and 497 nm, respectively whereas their emission maxima were observed at 524, 509, 560, 517 and 508 nm respectively. The corresponding organic nanoparticles (ONPs) showed peak broadening in their absorption and emission spectra. Further, the absorption and emission maxima of the ONPs where different as compared to the respective molecules and the fluorescence intensity of all ONPs were significantly lower. These spectral features indicate aggregation of the BODIPY chromophores during ONP formation.

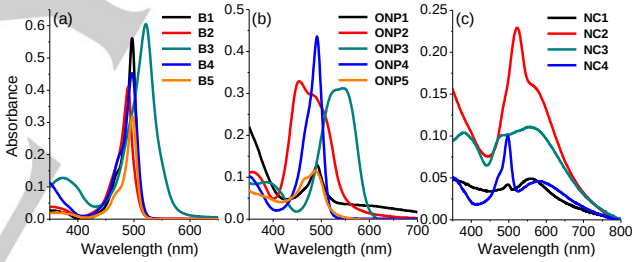


**Figure 2**. UV-Visible absorption spectra of (a) the BODIPY dyes **B1-B5** (11, 49, 31, 18 and 12 µM, respectively) in acetonitrile and (b) the organic nanoparticles **ONP1-ONP5** (93, 8.6, 9.2, 19 and 12 µM, respectively) in water and (c) the nanocomposites (**NC1-NC5)** (16 µg/mL each) in water.

The absorption spectra of the nanocomposites exhibited features that could be assigned to their constituents, i.e. the BODIPY molecules and the gold nanoparticles. However, it is important to note that the absorption spectra of the nanocomposites were not additive of the individual components. For instance, **NC1** showed two absorption peaks at 500 and 550 nm (Figure 2c and Table 1) which could be assigned to the electronic transitions in the BODIPY moiety and the SPR in gold nanoparticles, respectively. However, the peak width and position of these transitions were different as compared to **B1** and **Au NP**. Similar disparities were observed in the absorption spectra of **NC2**-**NC4** as compared to their constituents thereby indicating interaction between the BODIPY chromophore and gold within the nanocomposites.

It is known that BODIPY molecules are highly fluorescent in solution and their fluorescence is reduced in the aggregated state. Intriguingly, we observed that the fluorescence of the nanocomposites **NC1**-**NC3** was completely quenched (Figure

S12) whereas the emission of the nanocomposite **NC4** was similar to the chromophore **B4**. We attribute this to the chromophores **B4** that might have leached out of the nanocomposite due to its unstable nature. The complete quenching of fluorescence in **NC1**-**NC3** was surprising and detailed ultrafast measurements were carried out to elucidate the underlying mechanism (discussed below).

**Table 1**. Photophysical properties and photostability of the BODIPY molecules **B1**-**B5** in acetonitrile and the organic nanoparticles **ONP1**-**ONP5** and the nanocomposites **NC1**-**NC5** in water.

| Sample | $\lambda_{abs}$ [nm] | $\lambda_{em}$ [nm] | $\phi_f$ | Photostability | $\phi_\Delta$[‡] |
|---|---|---|---|---|---|
| **B1**[39] | 495 | 524 | 0.87 | No | nd |
| **B2**[40] | 490 | 509 | 0.95 | No | nd |
| **B3**[40] | 520 | 560 | 0.01 | Yes | 0.62 |
| **B4**[41] | 496 | 517 | 0.025 | No | nd |
| **B5**[40] | 497 | 508 | 0.65 | No | nd |
| **ONP1** | 495 | 526 | nd | No | nd |
| **ONP2** | 455, 488 | 515 | nd | No | nd |
| **ONP3** | 530 (br) | 550 | nd | No | nd |
| **ONP4** | 490 | 499 | nd | Yes | 0.28 |
| **ONP5** | 487 (br) | 506 | nd | No | nd |
| **NC1** | 497, 550 | † | † | Yes | 0.46 |
| **NC2** | 520, 566 | † | † | Yes | 0.12 |
| **NC3** | 450-800 (br) | † | † | Yes | 0.42 |
| **NC4** | 498, 557 | 514 | nd | No | nd |

[‡], singlet oxygen quantum yield determined using methylene blue as the reference standard; [nd], not determined; [†], no observable fluorescence.

Next, we were interested in estimating the quantity of BODIPYs that were incorporated in the nanocomposites by extracting the dyes from the nanocomposites. As reported earlier, we observed that **B1** was incorporated quantitatively in **NC1** and the amount of **B1** was estimated to be 0.96 mM. Owing to the strong interaction between **B1** and gold, we had used cysteine as a competing ligand for displacing **B1** from **NC1**.[35,42] However, for the nanocomposites **NC2**-**NC4**, we were able to extract the dyes through a simple solvent extraction using dichloromethane (DCM). Subsequent UV-Vis absorption spectral analysis of the extracted DCM part showed that 0.79, 0.76 and 0.4 mM of **B2**-**B4** were incorporated in **NC2**-**NC4**, respectively (Figure S13) which amounts to 21, 24 and 0.6% with respect to the concentration with which the nanocomposite synthesis was initiated. The enormous difference in the dye loading capacity of **NC1** as compared to **NC2**-**NC4** substantiates the role of structural features in stabilizing the nanocomposites.

NMR spectroscopy was then used to establish the chemical constitution of the nanocomposites and to assess the binding strength between the components. It was observed that the aliphatic protons $H_c$ and $H_d$ of tryptophan showed downfield shifts of $\Delta\delta$ 0.30 and 0.10 ppm, respectively, after being accommodated in **Au NP** whereas the aromatic protons ($H_{e\text{-}j}$) showed negligible shifts under the same conditions (Figure 3a,b). On the other hand, the aliphatic proton $H_c$ of tryptophan appeared upfield in **NC1** as compared to **Au NP** whereas the aromatic protons $H_{e\text{-}j}$ appeared downfield (Figure 3b,c). In **NC2** and **NC3**, the chemical shift position of the aliphatic proton $H_c$ was intermediate to **Au NP** and **NC1** whereas the aromatic protons ($H_{e\text{-}j}$) were significantly downfield shifted (Figure 3d,e).

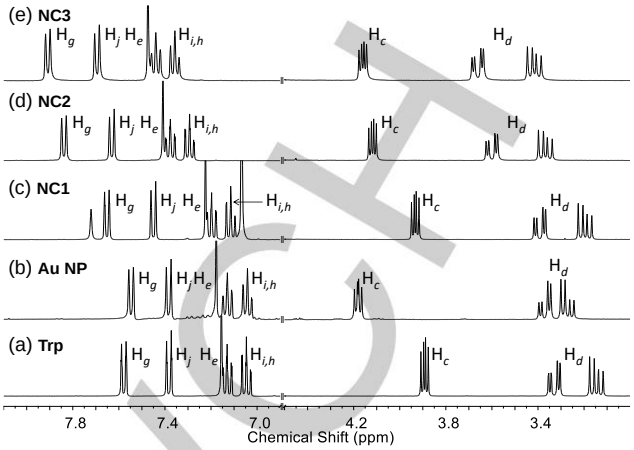


**Figure 3**. $^1$H NMR spectra of (a) tryptophan (**Trp**), (b) **Au NP**, and (c-e) the nanocomposites **NC1**-**NC3** in $D_2O$.

On the basis of the NMR data, we propose a model for the nanocomposites as shown in Figure S14. It is inferred that the composition of the nanocomposites is complex and a synergism of multiple non-covalent interactions stabilize the nanocomposites. The observation of downfield shift for $H_c$ in **Au NP** as compared to **Trp** suggests that the side chain of the tryptophan moiety is bound strongly to gold in **Au NP** whereas the aromatic rings interacted minimally. In **NC1**, the position of $H_c$ is similar to that in **Trp** which indicates that tryptophan moieties are displaced by **B1** thereby implying strong interaction of **B1** with gold. We had reported significant changes in the $^{19}$F NMR spectrum of **NC1** as compared to **B1** which substantiates strong interaction of **B1** with gold.[35] Further, it is proposed that hydrogen bonds are formed between the aromatic –NH of the tryptophan and a fluorine atom of the $–BF_2$ unit of **B1**. The observed downfield shifts in the aromatic region could thus be the result of a combination of hydrogen bonding, π-π stacking and CH-π interactions between the BODIPY core and the indole ring of tryptophan. The intermediate position of $H_c$ in **NC2** and **NC3** as compared to **Au NP** and **NC1** suggests that the interaction between **B2** and **B3** with gold is weak because of their steric bulkiness and hydrophobicity imparted by the methyl groups on the BODIPY core. The downfield shift of the aromatic protons of **NC2** and **NC3** on the other hand indicates strong interaction between the methyl groups of the BODIPY with the aromatic ring of tryptophan. The varying steric bulkiness and the hydrophobicity of the BODIPY molecules thus defines the binding strength of the BOIDPYs to gold through supramolecular interactions eventually resulting nanocomposites with varying stabilities.

After establishing the composition and strength of the nanocomposites, we were interested in evaluating their photostability and photosensitization properties of the nanocomposites which are crucial for applications in photodynamic therapy (PDT). The photostability of the molecules, ONPs and nanocomposites was evaluated by monitoring the changes in the absorption spectra of their solution after irradiation under a Xenon arc lamp for 10 minutes. We observed that the absorbance of **B3**, **ONP4**, **NC1**, **NC2** and **NC3** was unaffected upon irradiation thereby demonstrating their excellent photostability (Table 1 and Figures S15-S17). However, under

similar conditions the absorbance of other systems decreased considerably thus indicating photo-bleaching.

The ability of nanocomposites to photosensitize the generation of singlet oxygen was studied using 1,3-diphenylisobenzofuran (DPBF) as a singlet oxygen trapping agent. It is known that DPBF reacts with singlet oxygen rapidly and the progress of the reaction can be monitored by UV-Vis absorption spectroscopy. An aqueous solution of a mixture of DPBF and the nanocomposites were photo-irradiated and the changes in the UV-Vis absorption spectrum was monitored. As shown in Figures 4, S18 and S19, we observed a decrease in the absorbance at 420 nm upon irradiation which indicates the photooxidation of DPBF. However, the rate of the reaction varied for each nanocomposite and served as a parameter to assess the efficiency of singlet oxygen generation. Further, the quantum yield for singlet oxygen generation ($\phi_\Delta$) was calculated by using methylene blue as a reference standard and the data are presented Table 1. It is noteworthy that the singlet oxygen quantum yield of **NC1** and **NC3** were reasonably high (0.46 and 0.42, respectively) and were comparable to that of methylene blue (Figure S20). It was also observed that **Au NP** was capable of generating singlet oxygen under similar conditions but the singlet oxygen quantum yield was significantly lower ($\phi_\Delta$ = 0.027).[35]

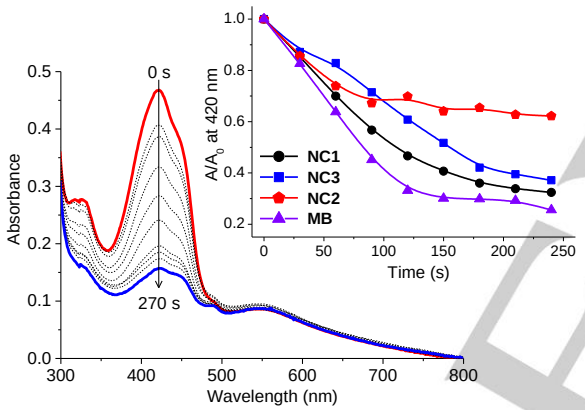


**Figure 4**. Changes in the UV-visible absorption spectrum of a solution of 1,3-diphenylisobenzofuran (DPBF, 65 µM) and the nanocomposite **NC1** (16 µg/mL) in 5% ethanol-water mixture. Inset shows the relative changes in absorbance at 420 nm of a solution of DPBF (65 µM) in the presence of methylene blue (**MB**, 65 µM) and the nanocomposites **NC1-NC3** (16 µg/mL) in 5% ethanol-water mixture.

In pursuit of an appropriate explanation for the distinct singlet oxygen generation efficiency of these systems and realizing the native photophysical behavior in the gold-molecule hetero-system, transient absorption spectroscopy was employed. Figure 5a-c shows the transient evolution of the differential absorption spectra of **B1**-**B3** with 450 nm pump excitation. We observed a strong photoinduced bleach feature peaking around 505 nm in all the three systems corresponding to the spin allowed π-π* transitions from $S_0$ to $S_1$ state.[43,44]. In BODIPYs, the primary channel for the effective production of singlet oxygen is the population of triplet states through the singlet-triplet intersystem crossing (ISC) process. However, in the presence of gold plasmonic interference, the mechanism of singlet oxygen generation could be different in BODIPY-gold nanocomposites. This could be due to facilitation of the ISC process against fast relaxation of $S_1$ to $S_0$[45] or because of the plasmonic photoexcitation induced population increment in oxygen singlet states.[46]

The transient absorption spectra of the nanocomposites **NC1**-**NC3** were dominated by gold plasmonic bleach signal around 540 nm (Figure 5d-f) thereby indicating a strong resonance coupling within gold nanoparticles and the molecular entities.[19,44] The plasmonic bleach signal in the nanocomposites was significantly red shifted as compared to the plasmonic bleach in gold nanoparticles (**Au NP**) photoexcited under similar conditions (Figure S21). It is noteworthy that a strong photoinduced absorption replaces the BODIPY ground state bleach feature in the spectra of the nanocomposites. This plausibly suggests a BODIPY to metal charge transfer phenomena in the nanocomposites. Quenching of the steady state fluorescence of BODIPYs while incorporated into the nanocomposites (Figure S12) also supports this inference. Henceforth, the possible mechanism behind singlet oxygen generation of the BODIPY-gold nanocomposites would be gold mediated photoexcitation of electrons into the high energy singlet states of oxygen. The fast relaxation of plasmonic excitations in gold nanoparticles (**Au NP**) inhibits the electron transfer process and results in poor singlet oxygen efficiency.[46] In the case of nanocomposites, it is hypothesized that the longer lifetime of plasmonic excitations resulting from the migration of photoexcited BODIPY electrons provide a longer time window for the electron transfer into the oxygen singlet states.

To realize the intensity of gold-BODIPY coupling in different systems we analyzed the bleach dynamics of pure molecular systems and their respective gold nanocomposites as a function of pump-probe delay time (Figure 6). The growth and decay profiles of **B1**-**B3** suggested a tentative prospect of electron transfer to gold. It was observed that the growth time of the ground state bleach was higher for **B1** as compared to **B2** and **B3** suggesting a longer relaxation time for **B1** (Figure 6a) thereby indicating the possibility of hot electron transfer in **NC1** which is very unlikely in **NC2** and **NC3**. The slower recovery kinetics of **B1** and **B2** would edge them over **B3** for the gold-molecule coupling resulting in efficient electron transfer to gold. Figure 6b shows the gold plasmon dynamics for **NC1**-**NC3** corresponding to the earlier described plasmonic bleach signals. Plasmon dynamics for pure gold nanoparticles (**Au NP**) are also plotted in Figure 6b for reference. The growth time of the plasmonic bleach gradually decreased from **NC1** to **NC3** though all three growth parameters were higher than the instantaneous rise in the case of **Au NP**. The growth time component of a plasmonic signal is the result of electron-electron scattering in photoexcited hot electron gas before they are thermalized in the SPR state.[47] Thus, an increase or decrease in the scattering time would refer to a change in electron population in the metal regime. According to our experimental results in Figure 6b, electron population in the metal excited states descends as **NC1** > **NC2** > **NC3** > **Au NP**. This would also stand for the coupling intensity in the nanocomposites and corroborates well with the gold-BODIPY interaction studied by NMR spectroscopy. It is hypothesized that a higher interaction probability of BODIPY readily enhances the plasmon lifetime thereby resulting in superior singlet oxygen population. However, the higher singlet oxygen efficiency of **NC3** as compared to **NC2** could be due broader plasmonic absorption of **NC3** as clearly seen in Figure 5f. It is also inferred that the heavy atom effect[48] of **B3** entity contributes towards the singlet oxygen generation in **NC3** along with the gold mediated phenomena owing to their poor gold-BODIPY interaction

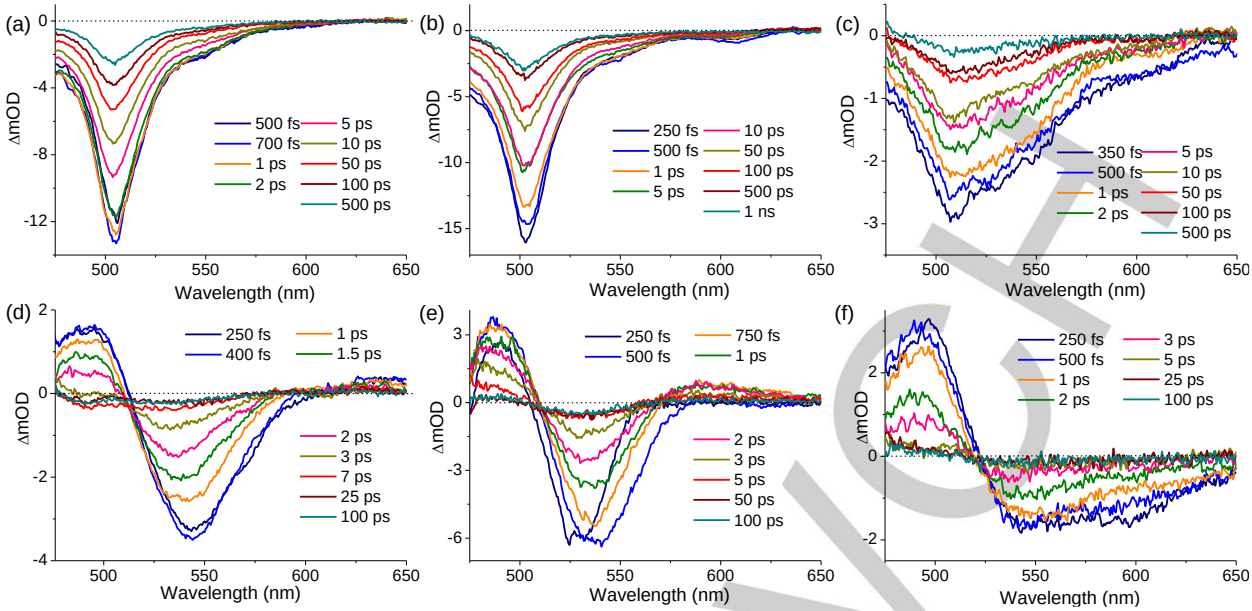


**Figure 5**. Transient absorption spectra of (a-c) the BODIPY molecules **B1**-**B3** in acetonitrile, and (d-f) the nanocomposites **NC1**-**NC3** in water as a function of pump-probe delay time for 450 photoexcitation. [**B1**], 11 μM; [**B2**], 49 μM; [**B3**], 31 μM; [**NC1**-**NC3**], 16 μg/mL each.

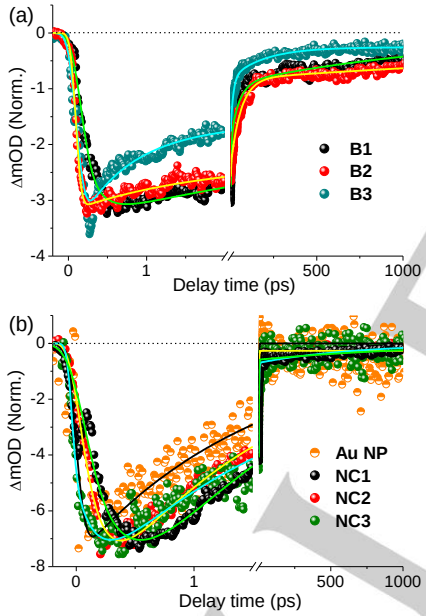


**Figure 6**. Transient kinetic profiles portraying comparative kinetics of (a) **B1**-**B3** and (b) **NC1**-**NC3** after 450 photoexcitation.

We propose a simplified scheme to discuss gold mediated photoinduced processes in **NC1** and **NC2** (Figure 7). We could differentiate them based on our experimental analysis citing discrepancy in their photophysical processes. In the presence of gold, photoexcited BODIPY electrons are transferred into the metal SPR states or occupy the unfilled *6sp* band with subsequent intra-band relaxation. This would slow down the fast relaxation of plasmonic electrons and enhance the gold carrier lifetime which is crucial for extraction of electrons to fill up the singlet states of oxygen. The observed emergence of molecular bleach signal in the transient spectra of **NC1** after 3 ps indicates the refilling of the $S_1$ state through back-electron transfer from gold to **B1**, though, in the early time scales (≤ 3 ps) it was covered by gold hot electron absorption. The intensity of the bleach was observed to be very weak as compared to pure BODIPYs thereby indicating a poor carrier population in the state so that back-migration of the transferred electrons towards $S_1$ is massively hampered which in turn helped in populating the singlet state of oxygen. For **NC2**, hot electron transfer would be minimal because of fast relaxation of the photoexcited electrons in the molecular regime and BODIPY-gold electron transfer would be probable only from the near band edge states. Referring to our experimental results on singlet oxygen efficiency, one may conclude that hot electron transfer to be the most effective channel for the delocalization of molecular electrons into gold owing to strong gold-BODIPY interaction, resulting in commendable singlet oxygen yield.

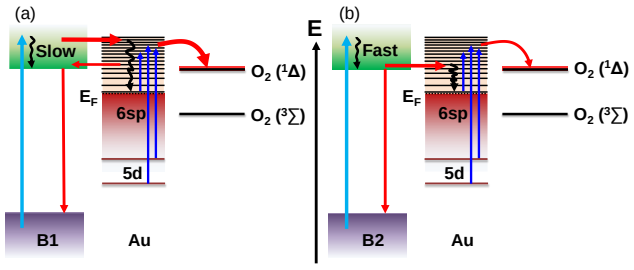


**Figure 7**. Schematic display of the excited state photophysical processes in (a) **NC1** and (b) **NC2** after 450 nm pump excitation resulting in generation of singlet oxygen.

## Conclusion

In conclusion, we have synthesized a series of water-soluble supramolecular nanocomposites containing BODIPY and gold nanoparticles via a simple synthetic procedure. The stability and strength of the nanocomposites were studied by NMR

spectroscopy and it was observed that an increase in steric bulkiness and hydrophobicity of the BODIPY molecules destabilized the nanocomposites. Interaction of the SPR on gold nanoparticles and BODIPY molecules significantly altered their photophysical properties and aided the generation of singlet oxygen. Ultrafast spectroscopy studies revealed that the plasmonic photoexcitation of gold nanoparticles in the nanocomposites was responsible for the efficient generation of singlet oxygen. It was noticed that hot electron transfer from BODIPY to gold was maximum in the case of **NC1** due to their slow photorelaxation process within the molecular regime. This migration of hot electrons from BODIPY to gold nanoparticles upon the plasmon photoexcitation resulted in the efficient generation of singlet oxygen for **NC1**. For **NC3** the heavy atom effect along with a broad plasmonic absorption helped in the generation of singlet oxygen. This study thus showcases the importance of molecular structure on the photophysical properties of supramolecular nanocomposites and can aid in the fabrication of nanoplasmonic systems for photodynamic therapy, solar cells, photocatalysis and nanophotonics.

## Experimental Section

**General Techniques**. All experiments were carried out at room temperature (25 ± 1 ºC) unless otherwise mentioned. NMR spectra were measured on a 400 MHz Bruker Avance II 400. Chemical shifts are reported in parts per million ($\delta$) calibrated using tetramethyl silane as an internal standard for samples in $CDCl_3$ and [$D_6$]DMSO, and to the residual solvent signals at $\delta$ 4.79 ppm for samples in $D_2O$. HR-TEM images were acquired on a Jeol 2100 HR operating at 120 kV. Samples were prepared by depositing a drop of diluted nanoparticle suspension on 300 mesh TEM grid and dried under vacuum for 2 hours. Dynamic light scattering experiment was performed using Malvern Zetasizer 2000 DLS spectrometer with 633 nm CW laser. The particles were dispersed in Milli Q water before analysis. Photosensitization experiments were carried out using a 400 W Xenon arc lamp (Oriel instruments) with a 475 nm cutoff filter (Newport Corporation). Absorption spectra were recorded on a Shimadzu UV-Vis spectrophotometer in 3 mL quartz cuvettes having a path length of 1 cm. Fluorescence spectra were recorded on a fluorolog 3-221 fluorimeter equipped with 450 W Xenon lamp.

**Femtosecond transient absorption spectroscopy.** We used a Ti:sapphire amplifier system (Astrella, Coherent) and a Helios-Fire spectrometer as described in our recent article.[49] Pump line passes through Optical Parametric Amplifier (OPerA-SOLO) to produce 450 nm pulses, used for sample excitation. Monochromatic probe pulses are converted into white light continuum employing a sapphire crystal. The probe beam is focused on the sample, overlapped with the pump and detected using CMOS detectors connected with the computers. Surface explorer software was used to analyse and fit the transient data.

**Materials**. Pyrrole, 2,4-dimethyl pyrrole and boron trifluoride diethyl etherate, were purchased from Alfa Acer. $HAuCl_4$, benzoyl chloride and 1,3-diphenylisobenzofuran (DPBF) were purchased from Sigma-Aldrich. Acetyl chloride, L-tryptophan, silica gel (60-120 mesh), acetone, dichloromethane, hexane and triethylamine were purchased locally. Solvents were distilled before use. Distilled water was used for all experiments.

**Synthesis of BODIPY B1 and B2**.[37,39] Freshly distilled pyrrole (0.48 mL, 7 mmol) or 2,4-dimethyl pyrrole (0.72 mL, 7 mmol) was dissolved in 100 mL dry dichloromethane and acetyl chloride (0.24 mL, 3.5 mmol) was added drop-wise under an atmosphere of nitrogen at 25 °C. The reaction mixture was then stirred for 12 hours at 25 °C. After cooling to 0 °C in an ice-bath, triethylamine (2.5 mL, 17.5 mmol) was added and stirred for 30 minutes. $BF_3.OEt_2$ (1.29 mL, 10.5 mmol) was then added and stirred for another 12 hours at 25 °C. The reaction mixture was washed with water (3 × 25 mL) and brine solution (20 mL), the organic layers were collected, dried over $Na_2SO_4$, filtered and evaporated to get a dark residue. The crude product was purified by column chromatography over silica gel using a mixture of dichloromethane and hexane to afford compound **B1** or **B2**.

**B1** (30% yield): $^1$H NMR ([$D_6$]DMSO, 298 K, 400 MHz) δ (ppm) 2.71 (s, 3H), 6.62-6.64 (m, 2H), 7.63-7.64 (d, 2H, $J$ = 4 Hz), 7.99 (s, 2H); GC-MS m/z calculated for $C_{10}H_{10}BF_2N_2$ $(M+H)^+$: 207.09, found: 207.10.

**B2** (24% yield): $^1$H NMR ($CDCl_3$, 298 K, 400 MHz) δ (ppm) 2.41 (s, 6H), 2.52 (s, 6H), 2.58 (s, 3H), 6.05 (s, 2H), GC-MS m/z calculated for $C_{14}H_{17}BF_2N_2$ $(M)^+$: 262.15, found: 262.10.

**Synthesis of BODIPY B3**.[37] To a solution of **B2** (50 mg, 0.19 mmol) in dry $CH_2Cl_2$ (10 mL) *N*-iodosuccinimide (257 mg, 1.14 mmol) was added and the reaction was stirred under an atmosphere of nitrogen at 25 °C for 3 hours. The reaction mixture was then washed with water (3 × 25 mL) and brine solution (20 mL), the organic layers were collected, dried over $Na_2SO_4$, filtered and evaporated to get a pink residue. The crude product was purified by column chromatography over silica gel using a mixture of dichloromethane and hexane to afford compound **B3** in 82% yield. $^1$H NMR ($CDCl_3$, 298 K, 400 MHz) δ (ppm) 2.44 (s, 6H), 2.57 (s, 3H), 2.64 (s, 3H), 2.78 (s, 3H); GC-MS m/z calculated for $C_{14}H_{15}BF_2N_2I_2$ $(M)^+$: 513.90, found: 513.83.

**Synthesis of BODIPY B4 and B5**.[36,38,39] Freshly distilled pyrrole (0.5 g, 7.45 mmol) or 2,4-dimethyl pyrrole (0.5 g, 5.25 mmol) and benzoyl chloride (0.37 g, 2.63 mmol) were dissolved in 150 mL dry DCM, and the reaction mixture was stirred for 16 hours at room temperature. After cooling the reaction mixture to 0 °C, triethylamine (3 mL) was added and stirred for 5 minutes followed by the addition of $BF_3{\cdot}OEt_2$ (2 mL). The reaction mixture was allowed to warm up to room temperature, and stirring was continued for 4 hours. The reaction mixture was then washed with water thrice (15 mL each), organic layer was collected and dried over sodium sulphate. The solvent was evaporated off using a rotary evaporator, and the product was purified by column chromatography on silica gel (60-120 mesh) using a 1:1 mixture of hexane and DCM to afford the product.

**B4** (15 % yield): $^1$H NMR ($CDCl_3$, 400 MHz, 298 K) δ (ppm) 6.55 (2H, d, $J$ = 4 Hz), 6.94 (2H, d, $J$ = 4 Hz), 7.52-7.61 (5H, m), 7.95 (2H, s); GC-MS m/z calculated for $C_{15}H_{11}BF_2N_2$: 268.09, found: 268.16.

**B5** (18% yield): $^1$H NMR ($CDCl_3$, 400 MHz, 298 K) δ (ppm) 1.37 (6H, s), 2.56 (6H, s), 5.98 (2H, s), 7.26-7.29 (2H, m), 7.47-7.49 (3H, m); GC-MS m/z calculated for $C_{19}H_{19}BF_2N_2$: 324.16, found: 324.10.

**General synthesis of nanocomposites NC1-NC5**. To a stirred solution of L-tryptophan (25 mM) in 10 mL water at 25 °C, an aqueous solution of $HAuCl_4$ was added (1 mL from a 5 mM stock solution) followed by a solution of **B1-B5** in acetone (1 mL from a 5 mM stock solution). The solution which turned brown-orange upon mixing was stirred for 16 hours at 25 °C. The precipitated residue was collected after centrifugation, washed with water (3×1 mL), dried, and re-dispersed in water. The formation of nanocomposites was monitored through UV-Vis absorption measurements and were characterized by dynamic light scattering (DLS) and microscopy measurements.

**General synthesis of organic nanoparticles ONP1-ONP5**. ONPs were synthesized by the re-precipitation method. To 10 mL of distilled water, 1 mL from a 5 mM stock solution of **B1-B5** in acetone was added, and the resulting suspension was stirred for 12 hours at 25 ºC. The reaction mixture was then centrifuged, the residue was collected, washed with water (3×1 mL), dried and re-dispersed in water. The formation of

nanoparticles was monitored through UV-Vis measurements and were characterized by DLS and microscopy measurements.

**Investigation of singlet oxygen generation**. Stock solutions of the photosensitizers and the reference standard methylene blue (MB) were prepared in water whereas a stock solution of DPBF was prepared in a 5% mixture of ethanol and water. 100 µL of an aqueous solution of the photosensitizer was taken in a cuvette to which 2.4 mL DPBF in 5% ethanol was added. After recording the absorbance, the solution was irradiated using a Xenon lamp with a 475 nm cut-off filter. The decrease in absorbance of DPBF at 420 nm was monitored at regular intervals.

**Determination of singlet oxygen quantum yield**. Singlet oxygen quantum yield was determined by following a reported procedure. The quantum yield was calculated with reference to MB in water which is reported to have a quantum yield of 0.52. Singlet oxygen quantum yield was calculated according to the equation:

$$\Phi_{\Delta}(\text{sample}) = \Phi_{\Delta}(\text{ref}) \times \frac{\text{m(sample)} \times \text{F(ref)}}{\text{m(ref)} \times \text{F(sample)}}$$

where *m* is the slope of the difference in the change in the absorbance of DPBF (at 420 nm) with irradiation time, and *F* is the absorption correction factor, which is given by $F = 1–10^{-OD}$.

## Acknowledgements

A. Rahman thanks University Grants Commission for a research fellowship and P. P. P. Kumar thanks Science and Engineering Research Board (SERB), New Delhi for National Postdoctoral Fellowship (PDF/2017/001221). H. N. Ghosh is grateful to Department of Science and Technology, Government of India for J. C. Bose fellowship (JCB/2018/000047) and SERB for a research grant (CRG/2019/000938). We thank INST, Mohali for financial support and Sophisticated Analytical Instrumentation Facility, Panjab University, Chandigarh for analytical facilities.

**Keywords:** Dyes/sensitizers • gold • nanostructures • photosensitization • supramolecular chemistry

[1] G. Barbillon, *Mater.* **2019**, *12*, 1502.
[2] J.-F. Li, C.-Y. Li, R. F. Aroca, *Chem. Soc. Rev.* **2017**, *46*, 3962–3979.
[3] T. Wang, C. A. Nijhuis, *Appl. Mater. Today* **2016**, *3*, 73–86.
[4] D. Conklin, S. Nanayakkara, T.-H. Park, M. F. Lagadec, J. T. Stecher, X. Chen, M. J. Therien, D. A. Bonnell, *ACS Nano* **2013**, *7*, 4479–4486.
[5] Y. B. Zheng, B. Kiraly, P. S. Weiss, T. J. Huang, *Nanomedicine (Lond)* **2012**, *7*, 751–770.
[6] H. Chen, T. Ming, L. Zhao, F. Wang, L.-D. Sun, J. Wang, C.-H. Yan, *Nano Today* **2010**, *5*, 494–505.
[7] N. T. Fofang, N. K. Grady, Z. Fan, A. O. Govorov, N. J. Halas, *Nano Lett.* **2011**, *11*, 1556–1560.
[8] W. Ni, Z. Yang, H. Chen, L. Li, J. Wang, *J. Am. Chem. Soc.* **2008**, *130*, 6692–6693.
[9] N. T. Fofang, T.-H. Park, O. Neumann, N. A. Mirin, P. Nordlander, N. J. Halas, *Nano Lett.* **2008**, *8*, 3481–3487.
[10] G. P. Wiederrecht, G. A. Wurtz, J. Hranisavljevic, *Nano Lett.* **2004**, *4*, 2121–2125.
[11] X. Wang, S.-C. Huang, S. Hu, S. Yan, B. Ren, *Nat. Rev. Phys.* **2020**, *2*, 253–271.
[12] A. B. Taylor, P. Zijlstra, *ACS Sensors* **2017**, *2*, 1103–1122.
[13] D.-K. Lim, K.-S. Jeon, H. M. Kim, J.-M. Nam, Y. D. Suh, *Nature Mater.* **2010**, *9*, 60–67.
[14] B. Sepúlveda, P. C. Angelomé, L. M. Lechuga, L. M. Liz-Marzán, *Nano Today* **2009**, *4*, 244–251.
[15] M. A. Noginov, G. Zhu, A. M. Belgrave, R. Bakker, V. M. Shalaev, E. E. Narimanov, S. Stout, E. Herz, T. Suteewong, U. Wiesner, *Nature* **2009**, *460*, 1110–1112.
[16] A. Kinkhabwala, Z. Yu, S. Fan, Y. Avlasevich, K. Müllen, W. E. Moerner, *Nat. Photonics* **2009**, *3*, 654–657.
[17] F. Stellacci, C. A. Bauer, T. Meyer-Friedrichsen, W. Wenseleers, S. R. Marder, J. W. Perry, *J. Am. Chem. Soc.* **2003**, *125*, 328–329.
[18] J. Jana, M. Ganguly, T. Pal, *RSC Adv.* **2016**, *6*, 86174–86211.
[19] H. Chen, L. Shao, K. C. Woo, J. Wang, H.-Q. Lin, *J. Phys. Chem. C* **2012**, *116*, 14088–14095.
[20] J. Zhao, L. Jensen, J. Sung, S. Zou, G. C. Schatz, R. P. Van Duyne, *J. Am. Chem. Soc.* **2007**, *129*, 7647–7656.
[21] K. L. Kelly, E. Coronado, L. L. Zhao, G. C. Schatz, *J. Phys. Chem. B* **2003**, *107*, 668–677.
[22] H. Yu, Y. Peng, Y. Yang, Z.-Y. Li, *npj Comput. Mater.* **2019**, *5*, 1–14.
[23] S. L. Yefimova, G. V. Grygorova, V. K. Klochkov, I. A. Borovoy, A. V. Sorokin, Y. V. Malyukin, *J. Phys. Chem. C* **2018**, *122*, 20996–21003.
[24] B. Laban, V. Vodnik, M. Dramićanin, M. Novaković, N. Bibić, S. P. Sovilj, V. M. Vasić, *J. Phys. Chem. C* **2014**, *118*, 23393–23401.
[25] M. Futamata, Y. Yu, T. Yajima, *J. Phys. Chem. C* **2011**, *115*, 5271–5279.
[26] Y. Chen, K. Munechika, D. S. Ginger, *Nano Lett.* **2007**, *7*, 690–696.
[27] G. A. Wurtz, P. R. Evans, W. Hendren, R. Atkinson, W. Dickson, R. J. Pollard, A. V. Zayats, W. Harrison, C. Bower, *Nano Lett.* **2007**, *7*, 1297–1303.
[28] I.-I. S. Lim, F. Goroleski, D. Mott, N. Kariuki, W. Ip, J. Luo, C.-J. Zhong, *J. Phys. Chem. B* **2006**, *110*, 6673–6682.
[29] H. Wang, H.-Y. Wang, H.-B. Sun, A. Cerea, A. Toma, F. D. Angelis, X. Jin, L. Razzari, D. Cojoc, D. Catone, F. Huang, R. P. Zaccaria, *Adv. Funct. Mater.* **2018**, *28*, 1801761.
[30] S. Balci, B. Kucukoz, O. Balci, A. Karatay, C. Kocabas, G. Yaglioglu, *ACS Photonics* **2016**, *3*, 2010–2016.
[31] F. Nan, Y.-F. Zhang, X. Li, X.-T. Zhang, H. Li, X. Zhang, R. Jiang, J. Wang, W. Zhang, L. Zhou, J.-H. Wang, Q.-Q. Wang, Z. Zhang, *Nano Lett.* **2015**, *15*, 2705–2710.
[32] M. Sukharev, T. Seideman, R. J. Gordon, A. Salomon, Y. Prior, *ACS Nano* **2014**, *8*, 807–817.
[33] Y.-W. Hao, H.-Y. Wang, Y. Jiang, Q.-D. Chen, K. Ueno, W.-Q. Wang, H. Misawa, H.-B. Sun, *Angew. Chem., Int. Ed.* **2011**, *50*, 7824–7828.
[34] M. Malicki, J. M. Hales, M. Rumi, S. Barlow, L. McClary, S. R. Marder, J. W. Perry, *Phys. Chem. Chem. Phys.* **2010**, *12*, 6267–6277.
[35] P. P. P. Kumar, P. Yadav, A. Shanavas, S. Thurakkal, J. Joseph, P. P. Neelakandan, *Chem. Commun.* **2019**, *55*, 5623–5626.
[36] W. Sheng, F. Lv, B. Tang, E. Hao, L. Jiao, *Chinese Chem. Lett.* **2019**, *30*, 1825–1833.
[37] A. Maity, A. Sarkar, A. Sil, S. B. B. N, S. K. Patra, *New J. Chem.* **2017**, *41*, 2296–2308.
[38] X.-Z. Wang, Q.-Y. Meng, J.-J. Zhong, X.-W. Gao, T. Lei, L.-M. Zhao, Z.-J. Li, B. Chen, C.-H. Tung, L.-Z. Wu, *Chem. Commun.* **2015**, *51*, 11256–11259.
[39] M. Zhang, E. Hao, Y. Xu, S. Zhang, H. Zhu, Q. Wang, C. Yu, L. Jiao, *RSC Adv.* **2012**, *2*, 11215–11218.
[40] W. Li, L. Li, H. Xiao, R. Qi, Y. Huang, Z. Xie, X. Jing, H. Zhang, *RSC Adv.* **2013**, *3*, 13417–13421.
[41] R. W. Wagner, J. S. Lindsey, *Pure Appl. Chem.* **1996**, *68*, 1373–1380.
[42] P. P. P. Kumar, N. Kaur, A. Shanavas, P. P. Neelakandan, *Analyst* **2020**, *145*, 851–857.
[43] W. Wu, H. Guo, W. Wu, S. Ji, J. Zhao, *J. Org. Chem.* **2011**, *76*, 7056–7064.
[44] F. M. Dumanoğulları, Y. Tutel, B. Küçüköz, G. Sevinç, A. Karatay, H. Yılmaz, M. Hayvali, A. Elmali, *J. Photochem. Photobiol., A Chem.* **2019**, *373*, 116–121.
[45] B. C. De Simone, G. Mazzone, W. Sang-Aroon, T. Marino, N. Russo, E. Sicilia, *Phys. Chem. Chem. Phys.* **2019**, *21*, 3446–3452.
[46] S. J. Chadwick, D. Salah, P. M. Livesey, M. Brust, M. Volk, *J. Phys. Chem. C* **2016**, *120*, 10647–10657.
[47] G. V. Hartland, *Chem. Rev.* **2011**, *111*, 3858–3887.
[48] X.-F. Zhang, X. Yang, *J. Phys. Chem. B* **2013**, *117*, 5533–5539.
[49] A. Shukla, G. Kaur, K. Justice Babu, N. Ghorai, T. Goswami, A. Kaur, H. N. Ghosh, *J. Phys. Chem. Lett.* **2020**, *11*, 15, 6344-6352.

## Entry for the Table of Contents

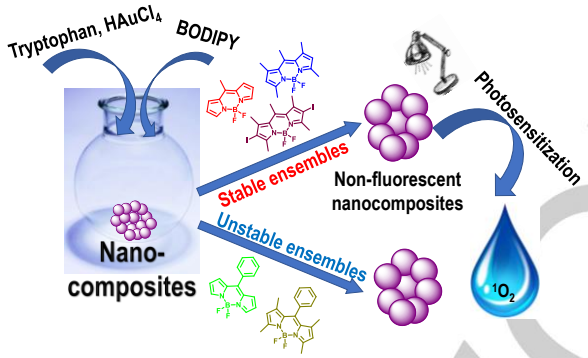


Hybrid nanostructures can be used for the design of functional optical devices and materials for various applications at the nanoscale. Supramolecular nanocomposites incorporating BODIPY dyes and gold nanoparticles were synthesized whose structural robustness and photophysical properties depended on the chemical structure of the constituent dye molecule.

Institute and/or researcher Twitter usernames: @ppn_inst, @INSTMohali